A novel approach to the production of NiCrAlY bond coat onto IN625 superalloy by selective laser melting

Jiwon Lee, Mathieu Terner, Etienne Copin, Philippe Lours, Hyun-Uk Hong

Additive Manufacturing 31 (2020) 100998

Contents lists available at ScienceDirect

Additive Manufacturing

journal homepage: www.elsevier.com/locate/addma

A novel approach to the production of NiCrAlY bond coat onto IN625 superalloy by selective laser melting

Jiwon Lee[a,b], Mathieu Terner[a], Etienne Copin[b], Philippe Lours[b,*], Hyun-Uk Hong[a,*]

[a] Department of Materials Science and Engineering, Changwon National University, 20 Changwondaehak-ro, Changwon, Gyeongnam 51140, Republic of Korea
[b] Institut Clément Ader (ICA), Université de Toulouse, CNRS, IMT Mines Albi, INSA, ISAE-SUPAERO, UPS, Campus Jarlard, F-81013 Albi, France

ARTICLE INFO

Keywords:
MCrAlY bond coat
Superalloy
Additive manufacturing
Powder bed fusion
Selective laser melting

ABSTRACT

The present study investigated for the first time the feasibility of producing by Selective Laser Melting (SLM) a NiCrAlY bond coat material directly onto an IN625 substrate itself produced by SLM. A typical parameters optimization was conducted by varying laser power (P) and scanning speed (v). Single-line scanning tracks and two-layer coatings were carried out and analyzed for 15 different P/v conditions. Several criteria were defined for the selection of appropriate SLM parameters. The results showed significant remelting of the underlying substrate, which is a typical feature of SLM manufacturing. This led to the formation of an intermediate dilution zone characterized by substantial mixing between IN625 superalloy substrate and NiCrAlY bond coat suggesting excellent metallurgical bonding. Optimum processing conditions were found for P = 250 W and v = 800 mm/s. It produced a dense 242 µm thick bond coat including a 36% dilution zone. The SLMed < NiCrAlY-IN625 > system exhibited a smooth microhardness profile slightly increasing from 275 Hv in the bond coat to 305 Hv in the substrate. A progressive Al concentration distribution between the phases and low residual stress levels were found in the system. This suggested that SLM might be a valuable alternative manufacturing process for bond coat systems promoting excellent adhesion for high temperature applications.

1. Introduction

Additive Manufacturing (AM) has become an outstanding alternative to conventional manufacturing, part of what is now commonly referred to as the 4th industrial revolution. AM presents many advantages such as versatility, complex and near-net-shape manufacturing, elimination of tooling, waste reduction, shorter lead time, etc. [1–3]. AM technologies have been classified into seven categories according to raw materials type, power source and processing technique [4]. For the production of metallic materials, Directed Energy Deposition (DED) and Powder Bed Fusion (PBF) are the most attractive and the most popular methods [1–6]. DED consists of direct deposition of material, usually spraying a powder simultaneously melted by a focused energy source through coaxial nozzles. Although the resolution is limited, these methods are particularly adapted to direct fabrication of rather simple shapes, cladding and remanufacturing/repair. By contrast, PBF consists in selective melting of powder layers by a focused power source, usually a laser or an electron beam. This allows the production of both internal and external complex geometries with much greater resolution therefore particularly suitable for direct manufacturing. There has been extensive research on these PBF technologies in particular for the fabrication of CoCr-Mo alloys, aluminum alloys and superalloys by Selective Laser Melting (SLM) for applications in aerospace, medical, automotive and power generation.

Ni-based superalloy Inconel 625 (IN625) is a popular material for gas turbine applications characterized by good high temperature strength, creep resistance, corrosion resistance and excellent weldability [7–10]. Due to this excellent weldability, fabrication of IN625 by SLM is particularly appropriate and has been properly optimized [11–14]. In order to enhance properties and increase operating temperatures of superalloys, Thermal Barrier Coating (TBC) have been developed to protect the substrates at high temperature so that they could retain their superior properties for longer time during operation [15–18]. Typically, TBCs provide insulation to enable superalloys to operate at about 150 °C above their usual upper limit [19–23]. These TBCs commonly consist in an external ceramic top coat (TC) for thermal insulation and an intermediate MCrAlY metallic bond coat (BC, where typically M = Ni, Co, Fe or a combination of those) to accommodate the difference in coefficient of thermal expansion between TC and superalloy substrate, and to grow a thin, compact and adherent protective oxide scale promoting optimized hot corrosion resistance [19–24].

As opposed to conventional casting and forging for substrate metals,

* Corresponding authors.
E-mail addresses: huhong@changwon.ac.kr (H.-U. Hong), philippe.lours@mines-albi.fr (P. Lours).

https://doi.org/10.1016/j.addma.2019.100998
Received 14 August 2019; Received in revised form 27 November 2019; Accepted 9 December 2019
Available online 11 December 2019
2214-8604/

these protective layers are generally coated onto the substrate by different conventional methods such as air or vacuum plasma spray (APS/VPS), electron beam-physical vapor deposition (EB-PVD) and arc ion plating (AIP) [20,21]. These separated processes require much manpower, cost and time. In addition, when coatings are conventionally applied, especially by plasma spraying, substantial residual stresses may be induced in the deposits, notably at the substrate-coating interface. This can generate delamination which is also a critical concern [25,26]. For these considerations, SLM of NiCrAlY bond coat onto IN625 substrate, itself produced by SLM, is considered in the present study. We believe that due to the nature of the SLM process, and in particular the typical remelting of underlying layers, excellent bonding between substrate and BC could be achieved. Although the ultimate production of complex coated geometries, such as blades, is challenged by the nature of PBF technologies requiring deposition of an entire layer of powder, therefore presently limiting the deposition onto flat surfaces, this issue could very well be addressed for example by selective deposition of different powders within a single layer by multiple powder containing tanks. There have been several studies regarding multi-material processing by SLM, as for instance with stainless steel and copper alloys [27–29], composite material mixing two different powders [30,31], NiCrAlY cladding [32–34], developed methodology accepting SLM concept [35] and innovative additive manufacturing of a steel-ceramic multi-material [36]. However, this is the first time to the best of our knowledge that SLM is used to produce both the superalloy substrate and the MCrAlY bond coat.

In the present paper, we study the optimization of SLM fabrication of a NiCrAlY bond coat onto an IN625 superalloy substrate, itself produced by SLM. The optimization of the process parameters is described on the basis of several criteria and the as-produced materials are thoroughly analyzed. We conclude with a set of processing conditions which shows very promising results. This suggests the feasibility of selective laser melting as an alternative method for the deposition of coatings in TBC systems.

2. Experimental procedure

2.1. Raw materials: pre-alloyed powders

The IN625 powder used in this study was a commercial gas-atomized pre-alloyed powder supplied by the SLM manufacturer SLM Solutions. The element composition of the powder, determined by inductively coupled plasma optical emission spectrometry (ICP-OES), is given in Table 1. The SEM micrograph in Fig. 1(a) shows the powder morphology: most powder particles were spherical with a small amount of irregular particles and aggregates. The powder size distribution was measured with a laser diffraction particle size analyzer (Malvern Mastersizer 3000). The particles had a size distribution between 20 µm (D_{10}) and 44 µm (D_{90}) with an average diameter of 29 µm (Fig. 1(c)). The powder flow rate was conveniently measured with a Hall flowmeter according to ASTM B213 standard and was 12.6 s. Such a powder with these characteristics is appropriate for SLM.

The main metallic element M for an MCrAlY bond coat generally depends on the substrate composition and is commonly Ni, Co or NiCo. To match the Ni-rich IN625 substrate, NiCrAlY was therefore selected in the present study (Table 1). Unconventional gas atomized NiCrAlY pre-alloyed powder with characteristics appropriate for SLM processing was specially ordered to Ducal International. The powder morphology was similar to that of IN625 with mostly spherical shape particles (Fig. 1(b)). The powder size distribution was measured between 24 µm (D_{10}) and 51 µm (D_{90}) with an average diameter of approximately 35 µm (Fig. 1(c)). The flowability was measured at 17.4 s. Although the particle size and flow time of the NiCrAlY powder were slightly higher than those of IN625, it is believed to have no significant influence on its processability by SLM since they remain in the processability window recommended by the manufacturer of the machine.

Table 1
Chemical composition in wt. % measured by ICP-OES of IN625 and NiCrAlY pre-alloyed powders used for SLM manufacturing.

	Ni	Cr	Mo	Fe	Co	C	Nb	Al	Y
Inconel 625	Bal.	20.08	8.27	3.49	0.6	0.08	3.12	0.35	–
NiCrAlY	Bal.	22.01	–	–	–	–	–	9.34	1.165

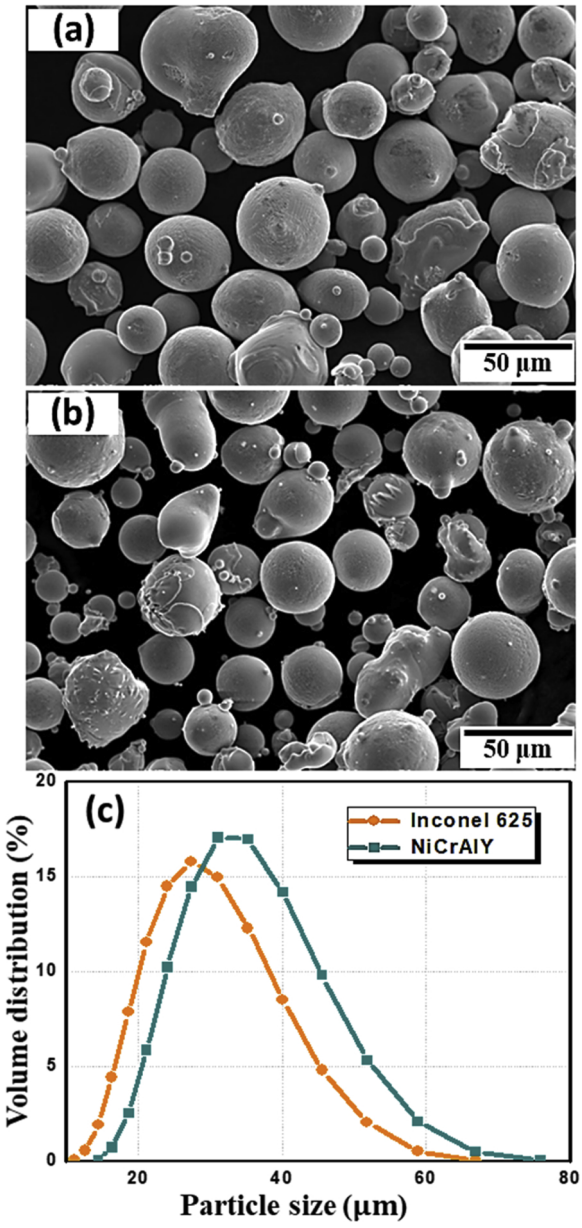

Fig. 1. SEM micrographs showing the (a) Inconel 625 and (b) NiCrAlY powders. (c) Particle size distribution showing the similarity of both powders.

2.2. SLM processing

The equipment used for additive manufacturing was an SLM 125 H L commercialized by SLM Solutions equipped with a 400 W Yb laser with a Gaussian beam focus diameter of 70 – 100 µm (constant in the present study for all processing conditions). The volume of fabrication allowed by the machine is 125 × 125 × 125 mm^3. The process was carried out under a protective argon atmosphere and the building platform was

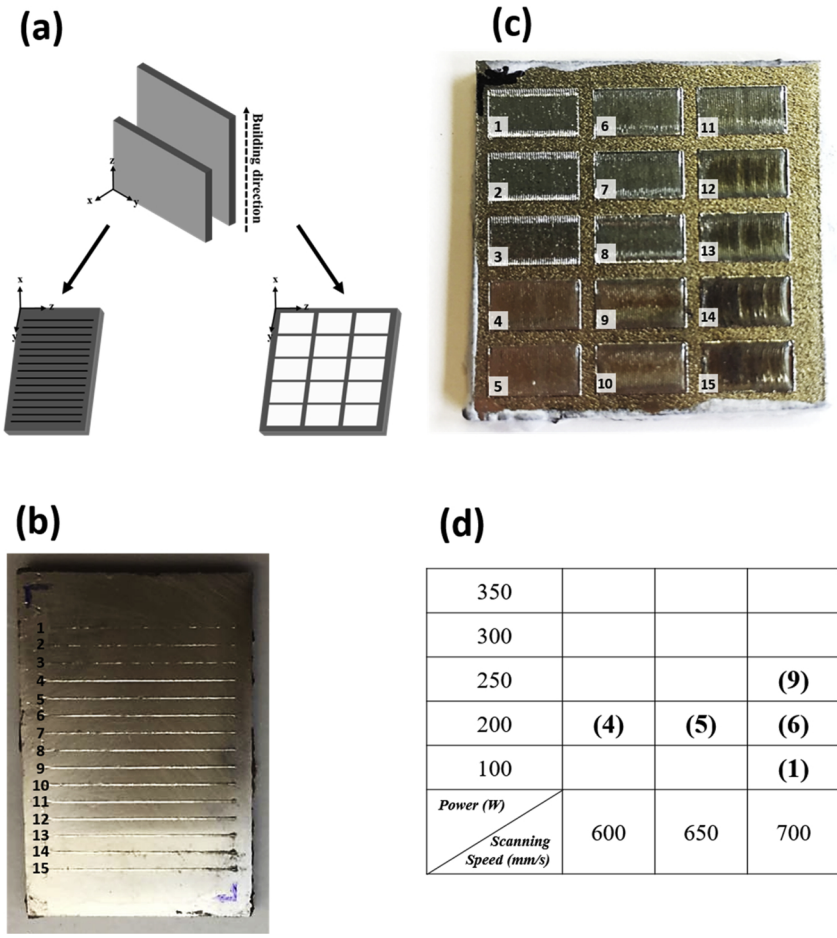

Power (W) / Scanning Speed (mm/s)	600	650	700	750	800
350				(14)	(15)
300				(12)	(13)
250			(9)	(10)	(11)
200	(4)	(5)	(6)	(7)	(8)
100			(1)	(2)	(3)

Fig. 2. (a) Schematics of the fabrication and experimental results of (b) single-line scanning tracks and (c) two-layer NiCrAlY coatings onto IN625 plate all produced by SLM according to *P/v* parameters conditions shown in (d).

held at 150 °C to reduce stress. Fabrication of IN625 by SLM has been studied and optimized extensively [11–14]. Due to its excellent weldability, this superalloy has been an interesting candidate for the early development of this technology. The processing conditions used for the fabrication of IN625 samples were: power P = 275 W, scanning speed v = 760 mm/s, hatch spacing h = 120 µm, layer thickness t = 50 µm. The scanning strategy includes contours and uses a stripes fill pattern type with stripes of length 10 mm and a rotation angle of the scanning directions of 33° between consecutive layers. These conditions, which could be further optimized, resulted in a residual porosity measured here below 0.5% considered more than acceptable for the purpose of the present study.

Two millimeters thick IN625 plates were built vertically to serve as substrate for subsequent NiCrAlY coatings (Fig. 2(a)). A 30 mm × 20 mm × 2 mm plate was polished down to grit 1200 SiC abrasive papers (Ra ≤ 20 nm) to remove the typical roughness resulting from SLM manufacturing measured at R_z = 37 ± 3 µm. This plate was used as the IN625 substrate for single-line NiCrAlY depositions (Fig. 2(b)) in order to evaluate track stability and bead geometry without artifacts due to roughness of the substrate base-plate otherwise substantial as well as to provide a clear contrast for optical analyses. Another as-built 30 mm × 30 mm × 2 mm plate, was used as-is as substrate for multi-layers NiCrAlY coating (Fig. 2(c)). After processing, plate's removal and thorough cleaning of the SLM machine, the IN625 superalloy substrate plates were fixed horizontally on the steel building platform using an OMEGABOND® OB-600 ceramic cement and a thermally conductive paste. The platform was then levelled so that the zero position would match the substrate plate surface for processing of the NiCrAlY coatings directly onto the IN625 substrates.

To the best of the aurthor's knowledge, there is not any reference in the literature about SLM processing of NiCrAlY. For this reason, the Granta CES EduPack™ 2017 database was used to identify typical SLM materials with physical and thermal properties close to that of NiCrAlY (melting point, thermal conductivity etc.), so as to use the set of parameters available in the literature for those materials as starting points for the parametric study. A process parameters optimization matrix was accordingly designed with 15 different values set of power *P* (W) and scanning speed *v* (mm/s) in reference to IN625 and CoCr-Mo alloys (Fig. 2(d)). The SLM process was conventionally carried out using a layer thickness of t = 50 µm, a hatch spacing of h = 120 µm, and scanning strategy similar to that of the IN625 substrate, though rotation between layers were not included. Single-line scanning NiCrAlY tracks, as in Fig. 2(b), were performed to analyze the track stability and bead or melt pool geometry. Furthermore, 8 mm × 4 mm NiCrAlY coatings consisting of two 50 µm layers were built, as in Fig. 2(c). Given the apparent density of the powder (approximately 60%) this theoretically corresponds to a coating thickness of about 70 µm, which is close to the typical thickness of MCrAlY bond coats in TBC systems [20].

2.3. Materials characterization

The single-line scanning tracks were cut perpendicular to the scanning direction to observe the bead or melt pool geometry in cross-section by optical microscopy. Top-views of the single-line scanning tracks were also taken by optical microscopy to measure more accurately the bead width and evaluate track stability. The two-layer coatings were cut perpendicular to the longitudinal direction, i.e. along the scanning direction. All specimens were then mounted and carefully

subjected to conventional metallographic preparation of grinding with abrasive SiC papers and fine polishing with diamond pastes down to 1 μm for observation by microscopy. The residual porosity of the SLMed NiCrAlY coatings was measured by microscopy according the ASTM standard E2109-01. Due to the small area of the BC, the porosity was measured systematically within the bond coat alone in five consecutive planes by grinding a few tens of micrometers, and averaged for each coating for statistical purpose. The microstructure was revealed by chemical etching with *aqua regia* solution and observed by optical microscopy (OM, Nikon EPIPHOT 200) and scanning electron microscopy (SEM, JEOL JSM-5800) equipped with energy dispersive X-ray spectroscopy (EDS). Kernel average misorientation (KAM) data acquired from electron backscattering diffraction (EBSD) with a field-emission scanning electron microscope (FE-SEM, MIRA-II) were used to measure local misorientation [37–41] and thereby assess qualitatively residual stress. To avoid artifacts from metallographic preparation, the final 1 μm polishing step was carried out using a colloidal silica suspension. Electron probe micro-analysis (EPMA, JEOL JXA-8100) was performed on unetched specimens to accurately determine the elemental distribution from the NiCrAlY bond coat surface to 300 μm in depth. Vickers microhardness (Mitutoyo HM-122) was measured every 40 μm from the top surface of the bond coat to 400 μm deep into the substrate for all conditions using a test load of 500 g.

3. Results and discussion

3.1. Single-line scanning analysis

Single-line scanning were processed, Fig. 2(b), in order to study the stability and geometry of the weld tracks for each condition. Although it was difficult to obtain conclusive results due to the instability of the weld track expected in SLM manufacturing and questioned representativity with respect to bulk processing due to the influence of processing adjacent tracks, these single-line scanning tracks were nevertheless found informative for preselection of the most appropriate processing conditions. Fig. 3 shows optical micrographs of the cross-section and the top-view of each single-line scanning track according to the different sets of power and scanning speed P/v. The bead or melt pool aspect was significantly different among all conditions.

As first consideration in Fig. 3, it was clear that remelting of the underlying IN625 substrate was substantial. This was evidenced by the measured values of geometrical dilution, as defined in Fig. 3, between 70 and as high as 90%. In cladding, the geometrical dilution should be as low as possible so as to have the composition of the bead close to the filler material. In conventional welding, gas metal arc welding (GMAW) for example, the geometrical dilution is often close to 50–60% [42]. Although SLM or PBF for that matter can arguably be assimilated to micro-welding, high geometrical dilution is typical due to remelting of underlying layers, leading to epitaxial columnar structures with grains elongated along the direction of the heat flux, that is perpendicular to the melt pools boundary [43]. Since bonding between superalloy substrate and MCrAlY bond coat is critical in TBC systems, this specificity is most certainly desirable.

The bead or melt pool shape was unclear due to this high amount of dilution and therefore very similar chemical composition and microstructure with the substrate. While for some conditions melt pools clearly exhibited the typical “fish scale” elliptical geometry often observed in SLM as-built materials (for example when $P = 100$ W), for others the melt pool resembled the typical “keyhole” shape characteristic of conventional welding (for example when $P = 250$ W). This keyhole shape is formed by the displacement of the melt induced by evaporation recoil pressure, while surface tension and hydrostatic pressure oppose cavity formation [44]. An advantage of the keyhole shape is to limit the heat affected zone (HAZ) [44,45]. This HAZ, which is generally characterized by locally heat affected grains and precipitates, is a weak part in welded material due to inhomogeneous microstructure and coarsened precipitates and grains. While subsequent laser melting of adjacent tracks significantly affects microstructure due to overlapping and remelting, limited HAZ is certainly more favorable. In Fig. 3, several melt pools seem to exhibit voids within the melt pool or at interface. These were artifacts from chemical etching, as confirmed by unetched conditions, and therefore not relevant. The bead or melt pool widths, indicated in Fig. 3, were also significantly affected by the processing conditions. A hatch spacing of 120 μm was selected for manufacturing the two-layer plates, and an overlapping between adjacent tracks of about 20–30% is usually desired for SLM [46]. For these reasons, a bead width between 150 and 180 μm was considered appropriate. As a result, with regards to melt pool geometry and width, laser powers of $P = 100$ W and $P = 350$ W incidentally corresponding to the lowest and highest energy density as defined in Fig. 3, respectively, were discarded.

3.2. NiCrAlY bond coat onto IN625 substrate

3.2.1. Morphology and hardness

Two-layer NiCrAlY 8 mm × 4 mm bond coats were successfully produced by SLM directly onto IN625 substrates using different parameters sets, as shown in Fig. 2(c). Macroscopically, the general aspect of the coatings is appropriate in most cases, except for laser powers of 100 and 350 W which were therefore not selected and will not be shown. This was consistent with the results of single-line scanning discussed in the previous section. Cross-section of the bond coats were evaluated and the corresponding optical micrographs are reported in Fig. 4 for all conditions. The thickness and porosity associated with different processing conditions were measured and reported in Fig. 4. The interface between substrate and bond coat could be comfortably identified thanks to the different building directions for substrate and bond coat. As first consideration, the micrographs in Fig. 4 highlight large voids or cavities at the edge of the coatings. This was caused by the considerable thermal contraction or shrinking during cooling, even causing the coatings to slightly bend upward at higher energy density. This is known as distortion caused by large thermal gradients in the workpiece [47]. Apart from that, bonding seemed excellent in all cases. Another surprising observation was that specimens produced with $P/v = 200/600$ and $P/v = 200/650$, which actually did not correspond to the lowest theoretical energy densities, exhibited the thinnest coatings with a thickness $\leq$ 75 μm. For the other conditions, all NiCrAlY bond coats appeared appropriate with a thickness between approximately 180 and 350 μm and low residual porosity $\leq$ 0.5%. The actual thickness of the coatings was significantly higher than the 100 μm thickness of the two NiCrAlY powder layers. Consistently with single-line scanning tracks observations in the previous section, this indicates that substantial remelting occurred. In fact, the micrographs in Fig. 4 suggest that rather than being deposited onto the IN625 substrate, the bond coat material is diluted into the superalloy substrate. This is most certainly valuable to ensure excellent bonding between bond coat and substrate.

Fig. 5 shows in more details the interface between bond coat and substrate. As mentioned above, this interface was clear due to the different building directions. The micrographs in Fig. 5 indicate that the bond coat was actually divided into two regions, clearly evidenced as a result of chemical etching. The brighter inner region was a dilution zone resulting from SLM of the first layer accompanied by significant remelting of the underlying IN625 substrate. The resulting material is a highly NiCrAlY/IN625 mixed zone. The darker outer region corresponded to the selective melting of the second NiCrAlY layer. There was as well significant remelting of the underlying layer, as evidenced by the effective thickness significantly larger than 50 μm. The presence of these dilution zones strongly suggests that SLM is highly appropriate. As opposed to conventional bond coat deposition methods such as PS and EB-PVD which typically exhibited a clear interface between bond coat and substrate often requiring a long diffusion heat treatment, the

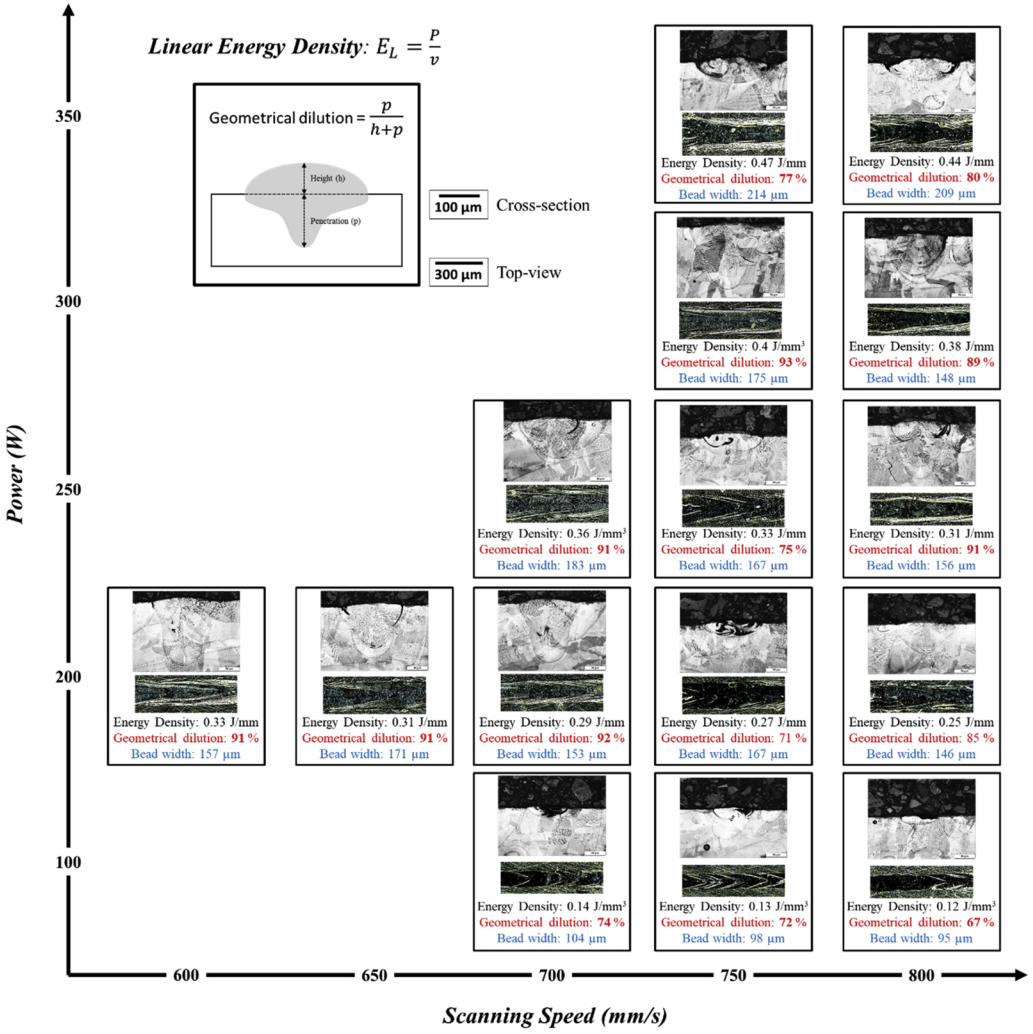

Fig. 3. Etched optical micrographs of the single-line scanning tracks showing the cross-section of the bead or melt pool and below the top view of the welding track for each processing condition. The corresponding values of energy density are reported as well as the measured values of geometrical dilution and bead width.

adhesion as a result of SLM processing appears to be excellent.

This was further evidenced by microhardness measurements from the top surface of the bond coat into the substrate, as reported in Fig. 5 for all conditions. Because of the similar chemical composition between NiCrAlY and IN625, the values of microhardness were similar as can be seen in Fig. 5. It was however found that the hardness was slightly higher in the substrate. This may result from the presence of Nb and Mo in solid solution in the as-built IN625 substrate. In the NiCrAlY bond coat, a gradual increase of hardness from the surface to the interface is observed, associated with the progressive chemical composition gradient. Hardness was often non-negligibly higher in the vicinity of the interface between substrate and bond coat corresponding to the heat affected zone. The hardness profile of the specimen produced with $P/v = 300/750$, corresponding to the highest energy density of 66.7 J/

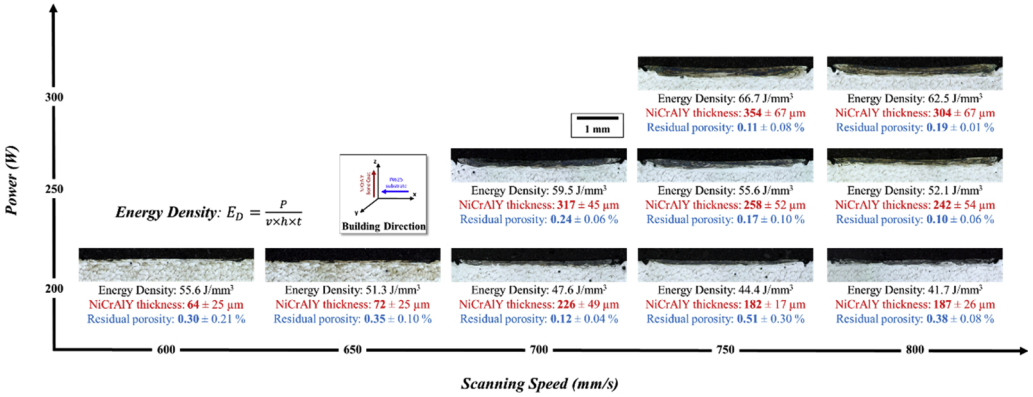

Fig. 4. Etched optical micrographs showing the cross section of the two-layer NiCrAlY coatings deposited onto IN625 substrate for each condition. The corresponding values of energy density are reported as well as the measured coating thickness and residual porosity.

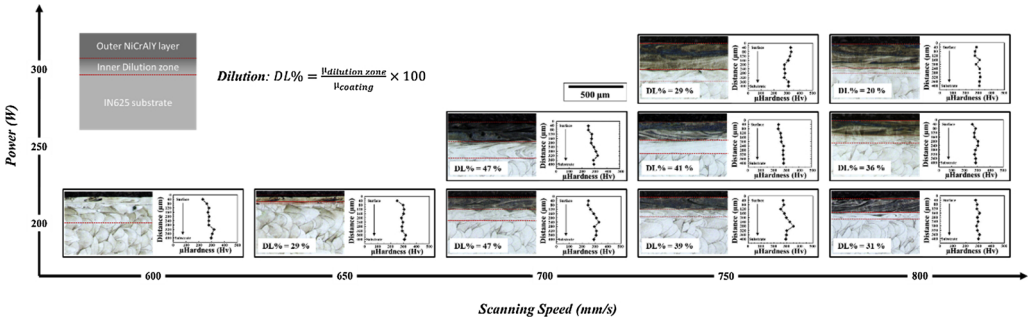

Fig. 5. Etched optical micrographs showing the details of the cross section of the two-layer NiCrAlY coatings deposited onto IN625 substrate for each condition. The dilution zones were highlighted and their values in % were reported. The micro hardness profile was included for each condition.

mm^3, indicated that hardness was significantly higher at the surface of the NiCrAlY bond coat. This suggests inhomogeneous phase distribution within the bond coat which may be detrimental to its performance. One of the critical function of MCrAlY bond coats in TBC systems is the accommodation of the significantly different coefficient of thermal expansion shown between the superalloy metallic substrate and insulating ceramic top-coat. To ensure appropriate bonding between substrate and bond coat, similar hardness between the two is preferred, particularly at the interface.

With considerations of thickness, residual porosity, dilution zone and hardness profile, the results exhibited in Figs. 4 and 5 allowed to proceed to a finer selection of the most appropriate processing conditions. Additionally, higher scanning speed is usually preferred in SLM manufacturing to promote faster solidification which prevents prejudicial segregation. In such light, NiCrAlY coatings produced with $P/v = 200/600$ and $P/v = 200/650$ were considered too thin. These conditions could therefore be eliminated. NiCrAlY coatings produced with $P/v = 200/700$ and $P/v = 250/700$ could also be discarded as there were no evident benefit in using lower scanning speed of 700 mm/s and the dilution zone was large above 45%. We therefore considered the most appropriate SLM processing to be $P/v = 200–300/750–800$ and selected these six conditions for further analyses. Under these conditions, NiCrAlY coatings had an appropriate thickness of approximately 180 ~ 350 μm including the dilution zone, a low residual porosity of 0.1 ~ 0.5% and a dilution of 20 ~ 40%.

3.2.2. Element distribution

One apparent advantage of considering SLM for coating NiCrAlY onto an IN625 substrate is the inherent remelting occurring during processing which generated what we called a dilution zone, as indicated and discussed in the previous section, suggesting excellent bonding between bond coat and substrate. Further evidence of this excellent combination was given by EPMA element distribution analyses, in particular the distribution of Al (Fig. 6). As indicated in Table 1, NiCrAlY shows a higher content of Al (9.34 wt.%) than IN625 (0.35 wt.%) to allow the growth of a stable protective Al_2O_3 layer at high temperature. The concentration profile of Al is therefore a key indicator of the interface position and the extent of the dilution zone between the substrate and the bond coat. In Fig. 6, the various regions of the NiCrAlY/IN625 system are clearly highlighted. The outer NiCrAlY was distinctly enriched with Al while the substrate exhibited low Al content. The dilution zones defined above were also clear with apparent mixing between bond coat and substrate. There was a clearly high Al concentration at the top of the NiCrAlY coating in all the cases, approximately 5 μm thick, likely due to the formation of a thin Al_2O_3 oxide layer. The micrographs in Fig. 6 most interestingly highlighted notable differences between processing conditions. With a laser power $P = 200$ W, the concentration of Al was significantly different between the regions showing clearly delimited layers. With a laser power $P = 250$ W, although the concentration profile of Al was certainly uneven, there was a more gradual variation and the interfaces were less pronounced.

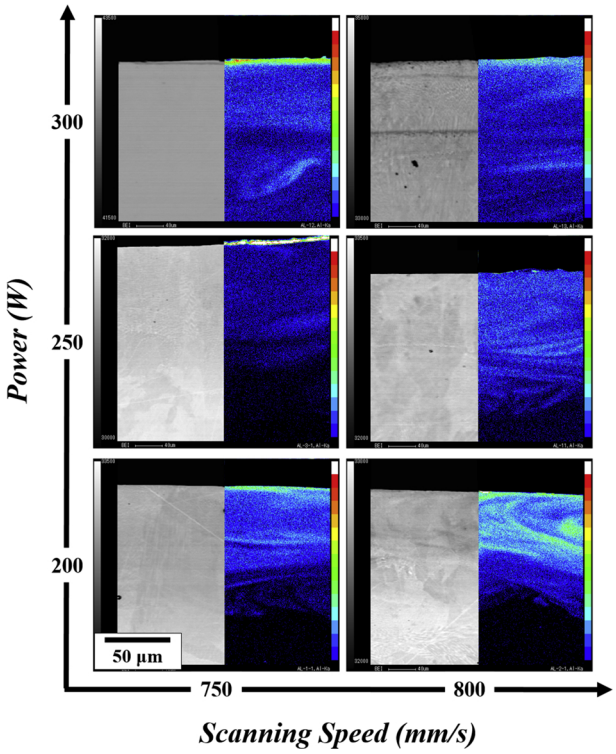

Fig. 6. EPMA results of aluminum content and corresponding backscattered electron imaging (BEI) micrographs showing the gradient of Al concentration (all scales are consistent). (For interpretation of the references to colour in this figure legend, the reader is referred to the Web version of this article.)

This was clearer with $P = 300$ W though the actual interface with the substrate was out of range (NiCrAlY thickness approximately ≥ 300 μm in Fig. 4).

EPMA results, although not decidedly conclusive, contribute to the appropriate selection of the optimum processing parameters. Excellent bonding is assumed by SLM due to appropriate mixing between the bond coat and the substrate to avoid clear interface between the two chemically different materials as observed in conventional APS/VPS or EB-PVD depositions. Most defects in these systems are evidenced by significant cracking at the interface during thermal cycles which often cause delamination and failure of the TBC. This is generally avoided to some extent by a long and costly diffusion heat treatment. The standard diffusion treatment for APS bond coat is 6 h at 1080 °C followed by 20 h at 870 °C [48]. Because the NiCrAlY coating processed by SLM advantageously exhibited the so-called dilution zone, such a diffusion treatment becomes unnecessary, at least for the purpose of inter-diffusion and adhesion. In such conditions, it appears that the NiCrAlY coating produced with $P/v = 250/800$ exhibiting a thickness of

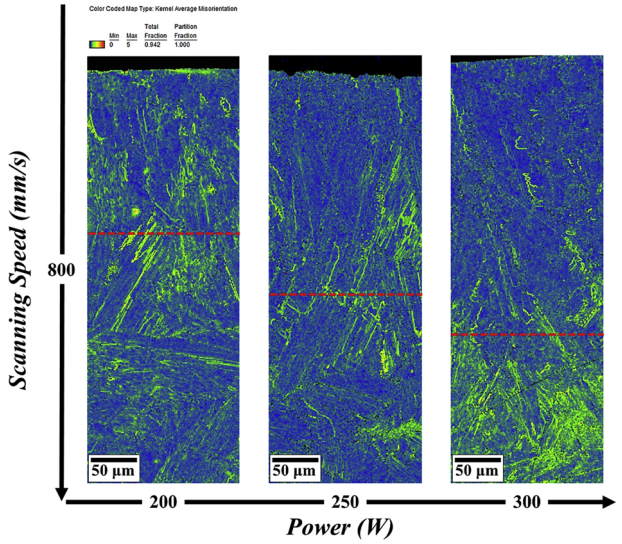

Fig. 7. Kernel Average Misorientation (KAM) maps highlighting residual stress levels. The interface between substrate and dilution zone was indicated by a dash line. (For interpretation of the references to colour in this figure legend, the reader is referred to the Web version of this article.)

approximately 250 µm including a roughly 35% dilution zone and low residual porosity about 0.1% seems most appropriate.

3.2.3. Residual stress

Kernel average misorientation (KAM) maps were generated from EBSD analyses. KAM is generally used for characterizing local misorientation. It calculates the average misorientation of a given point with all of its neighbors. This is a good qualitative indicator of deformed grain or strain induced grain, and therefore stress in crystalline materials at the microscale level. There are several reported methods for quantifying residual stresses in materials, which is particularly critical for SLM, such as the destructive hole-drilling method and the X-ray diffraction method [49]. Due to very fast solidification and cooling rates as well as multiple thermal cycles experienced during SLM processing, residual stress is often very high in the as-built materials as evidenced in particular by a high density of dislocations [11,50]. It is reasonable to assume that strain as measured by KAM maps in EBSD is due to residual stress built up during SLM processing, and therefore allows to qualitatively assess residual stress levels visually on a microscale at the expense of appropriately quantified values. Fig. 7 shows KAM maps for NiCrAlY coating produced with $P/v = 200/800$, $P/v = 250/800$ and $P/v = 300/800$. The evaluated interface corresponding to the interface between IN625 substrate and dilution zone as measured in Fig. 4 were included as dashed red lines in Fig. 7. Although the residual stress, amount of average misorientation, were qualitatively similar, as expected due to the very high solidification rate estimated around $10^5 \sim 10^6$ °C/s regardless of slightly different processing conditions [11], there were noticeable differences highlighted in Fig. 7.

For the NiCrAlY coating produced with $P/v = 300/800$, higher levels of misorientation were concentrated in the substrate in the vicinity of the interface with the bond coat. Further analyses need to be carried out to explain this behavior. However, it is reasonable to assume that higher energy density due to higher laser power generates more heat and therefore a larger heat affected zone within the unmelted substrate. Coatings produced with $P/v = 200/800$ and $P/v = 250/800$ exhibited relatively low levels of misorientation. Although more analysis is needed to assure the consistency of residual stress profile, the $P/v = 250/800$ condition showed the lowest stress levels and therefore the lowest risks of failure. For this reason, it was considered the most appropriate SLM condition for the production of NiCrAlY coating onto the IN625 substrate itself produced by SLM.

4. Conclusions

The present study investigated for the first time the feasibility of producing by SLM a NiCrAlY bond coat material onto an IN625 superalloy substrate, itself produced by SLM. Key contents are summarized as follows:

1 15 processing conditions were tested by varying the laser power between 100 and 350 W and the scanning speed between 600 and 800 mm/s. The results showed that in all cases, substantial dilution of the NiCrAlY layer into the IN625 substrate occurred due to the typical remelting characteristic of SLM manufacturing.
2 Several criteria were defined to determine the most appropriate processing conditions. An approximately 250 µm thick NiCrAlY coating is obtained with a very low residual porosity $\leq 0.1\%$ including a $\sim 35\%$ dilution zone, smooth hardness profile between 275 and 305 Hv, low residual stress levels and progressive Al concentration distribution for the following SLM processing conditions: layer thickness $t = 50$ µm, hatch spacing $h = 120$ µm, laser power $P = 250$ W and laser scanning speed $v = 800$ mm/s.
3 Future work will focus on a thorough characterization of this < NiCrAlY-IN625 > system produced by SLM in terms of composition, phase formation, mechanical properties and durability which will be appropriately compared to conventional systems produced by APS/VPS.

CRediT authorship contribution statement

Jiwon Lee: Conceptualization, Methodology, Validation, Formal analysis, Investigation, Writing - original draft. **Mathieu Terner:** Investigation, Writing - review & editing. **Etienne Copin:** Methodology, Writing - review & editing. **Philippe Lours:** Writing - review & editing, Supervision. **Hyun-Uk Hong:** Writing - review & editing, Supervision.

Declaration of Competing Interest

None.

Acknowledgment

The authors acknowledge the financial support of the Global Expert Technology Development Program grant funded by the Korean government (MOTIE, 10076876) and the National Research Foundation of Korea (NRF) grant funded by the Korean government (MSIP, NRF-2017R1A1A1A05000754 and NRF-2018R1A5A6075959).

References

[1] W.E. Frazier, Metal additive manufacturing: a review, J. Mater. Eng. Perform. 23 (2014) 1917–1928, https://doi.org/10.1007/s11665-014-0958-z.
[2] K.V. Wong, A. Hernandez, A review of additive manufacturing, ISRN Mechanical Engineering A 1 (2012), https://doi.org/10.5402/2012/208760.
[3] B. Baufeld, O.V. Biest, R. Gault, Additive manufacturing of Ti-6Al-4V components by shaped metal deposition: microstructure and mechanical properties, Mater. Des. 31 (2010) S106–S111, https://doi.org/10.1016/j.matdes.2009.11.032.
[4] ISO/ASTM 52900, ASTM International, The Global Leader in Additive Manufacturing Standards-The Committee on Additive Manufactruing Technologies (F42).
[5] ASTM International Committee F42 on Additive Manufacturing Technologies; Roland Berger.
[6] A. Lundb ä k, L.-E. Lingdgren, Finite element simulation to support sustainable production by additive manufacturing, Procedia Manuf. 7 (2017) 127–130, https://doi.org/10.1016/j.promfg.2016.12.033.
[7] L.M. Suave, J. Cormier, P. Villechaise, A. Soula, Z. Hervier, D. Bertheau, J. Laigo, Microstructural Evolutions During Thermal Aging of Alloy 625: Impact of Temperature and Forming Process, Metall. Mater. Trans. A (45A) (2014) 2963–2982, https://doi.org/10.1007/s11661-014-2256-7.
[8] S.J. Patel, G.D. Smith, The role of niobium in wrought superalloys, International Symposium Niobium 2001, Orlando, Florida, USA, TMS, 2001, pp. 1081–1102.
[9] D. Liu, X. Zhang, X. Qin, Y. Ding, High-temperature mechanical properties of Inconel-625: role of carbides and delta phase, Mater. Sci. Tech. 33 (2017)

1610–1617, https://doi.org/10.1080/02670836.2017.1300365.
[10] M.D. Mathew, P. Parameswaran, K. Bhanu Sankara Rao, Microstructural changes in alloy 625 during high temperature creep, Mater. Charact. 59 (2008) 508–513, https://doi.org/10.1016/j.matchar.2007.03.007.
[11] G. Marchese, M. Lorusso, S. Parizia, E. Bassini, J.W. Lee, F. Calignano, D. Manfredi, M. Terner, H.U. Hong, D. Ugues, M. Lombardi, S. Biamino, Influence of heat treatments on microstructure evolution and mechanical properties of Inconel 625 processed by laser powder bed fusion, Mater. Sci. Eng. A 729 (2018) 64–75, https://doi.org/10.1016/j.msea.2018.05.044.
[12] G. Marchese, X.G. Coera, F. Calignano, M. Lorusso, S. Biamino, P. Minetola, D. Manfredi, Characterization and comparison of Inconel 625 processed by selective laser melting and laser metal deposition, Adv. Eng. Mater. 19 (2016) 1–9, https://doi.org/10.1002/adem.201600635.
[13] S. Li, Q. Wei, Y. Shi, Y. Shi, Z. Zhu, D. Zhang, Microster-by-layer printing of laminated graphene-based interdigitatetured by Selective Laser Melting, J. Mater. Sci. Technol. 31 (2015) 946–952, https://doi.org/10.1016/j.jmst.2014.09.020.
[14] I. Koutiri, E. Pessard, P. Peyre, O. Amlou, T.D. Terris, Influence of SLM process parameters on the surface finish, porosity rate, and fatigue behavior of as-built Inconel 625 parts, J. Mater. Process. Technol. 255 (2018) 536–546, https://doi.org/10.1016/j.jmatprotec.2017.12.043.
[15] M. Daroonparvar, M.S. Hussain, M.A.M. Yajid, The role of formation of continues thermally grown oxide layer on the nanostructured NiCrAlY bond coat during thermal exposure in air, Appl. Surf. Sci. 261 (2012) 287–297, https://doi.org/10.1016/j.apsusc.2012.08.002.
[16] W. Leng, R. Pillai, P. Huczkowski, D. Naumenko, W.J. Quadakkers, Microstructural evolution of an aluminide coating on alloy 625 during wet air exposure at 900 °C and 1000 °C, Surf. Coat Tech. 354 (2018) 268–280, https://doi.org/10.1016/j.surfcoat.2018.09.043.
[17] F.A. Khalid, N. Hussain, A.H. Qureshi, Microstructural study on oxidation of aluminized coating on Inconel 625, J. Mater. Eng. Perform. 11 (2002) 211–214, https://doi.org/10.1361/105994902770344286.
[18] P.W. Schike, Advanced gas turbine materials and coatings, GE Energy, (2004).
[19] D.R. Clarke, M. Oechsner, N.P. Padture, Thermal-barrier coatings for more efficient gas-turbine engines, MRS Bull. 37 (2012) 891–898, https://doi.org/10.1557/mrs.2012.232.
[20] M. J. Donachie, S. J. Donachie, Superalloys: A Technical Guide 2nd ed. ASTM International, the Materials Information Society, ISBN: 0-87170-749-7.
[21] R. C. Reed, The Superalloys: Fundamentals and Applications, Cambridge University Press, ISBN: 978-0-511-24546-6.
[22] N.P. Padture, M. Gell, E.H. Jordan, Thermal barrier coatings for gas-turbine engine applications, Science's compass 296 (2002) 280–284, https://doi.org/10.1126/science.1068609.
[23] J.D. Osorio, A. Toro, J.P. Hernandez–Ortiz, Thermal barrier coatings for gas turbine applications: failure mechanisms and key microstructural features, DYNA 79 (2012) 149–158 http://www.scielo.org.co/scielo.php?script=sci_arttext&pid=S0012-73532012000600018&lng=en&nrm=iso.
[24] N. Zotov, M. Bartsch, L. Chernova, D.A. Schmidt, M. Havenith, G. Eggeler, Effects of annealing on the microstructure and the mechanical properties of EB-PVD thermal barrier coatings, Surf. Coat. Tech. 205 (2010) 452–464, https://doi.org/10.1016/j.surfcoat.2010.07.008.
[25] C.S. Richard, G. Beranger, J. Lu, J.F. Flavenot, The influences of heat treatments and interdiffusion on the adhesion of plasma-sprayed NiCrAlY coatings, Surf. Coat. Tech. 82 (1996) 99–109, https://doi.org/10.1016/0257-8972(95)02640-1.
[26] P.R. Chalker, S.J. Bull, D.S. Rickerby, A review of the methods for the evaluation of coating-substrate adhesion, Mat. Sci. Eng. A 140 (1991) 583–592, https://doi.org/10.1016/0921-5093(91)90482-3.
[27] Z.H. Liu, D.Q. Zhang, S.L. Sing, C.K. Chua, L.E. Loh, Interfacial characterization of SLM parts in multi-material processing: metallurgical diffusion between 316L stainless steel and C18400 copper alloy, Mater. Charact. 94 (2014) 116–125, https://doi.org/10.1016/j.matchar.2014.05.001.
[28] J. Chen, Y. Yang, C. Song, M. Zhang, S. Wu, D. Wang, Interfacial microstructure and mechanical properties of 316L/CuSn10 multi-material bimetallic structure fabricated by selective laser melting, Mat. Sci. Eng. A 752 (2019) 75–85, https://doi.org/10.1016/j.msea.2019.02.097.
[29] S.L. Sing, L.P. Lam, D.Q. Zhang, Z.H. Liu, C.K. Chua, Interfacial characterization of SLM parts in multi-material processing: intermetallic phase formation between AlSi10Mg and C18400 copper alloy, Mater. Charact. 107 (2015) 220–227, https://doi.org/10.1016/j.matchar.2015.07.007.
[30] A.G. Demir, B. Previtali, Multi-material selective laser melting of Fe/Al-12Si components, Manuf. Lett. 11 (2017) 8–11, https://doi.org/10.1016/j.mfglet.2017.01.002.
[31] C. Wei, L. Li, X. Zhang, Y.-H. Chueh, 3D printing of multiple metallic materials via modified selective laser melting, CIRP Ann. Manuf. Technol. 67 (2018) 245–248, https://doi.org/10.1016/j.cirp.2018.04.096.
[32] K. Partes, C. Giolli, F. Borgioli, U. Bardi, T. Seefeld, F. Vollertsen, High temperature behavior of NiCrAlY coatings made by laser cladding, Surf. Coat. Tech. 202 (2008) 2208–2213, https://doi.org/10.1016/j.surfcoat.2007.09.010.
[33] M.J. Tobar, J.M. Amado, A. Yanez, J.C. Pereira, C. Amigo, Laser cladding of MCrAlY coatings on stainless steel, Phys. Procedia 56 (2014) 276–283, https://doi.org/10.1016/j.phpro.2014.08.172.
[34] R. Vilar, E.C. Santos, P.N. Ferreira, N. Franco, R.C. da Silva, Structure of NiCrAlY coatings deposited on single-crystal alloy turbine blade material by laser cladding, Acta Mater. 57 (2009) 5292–5302, https://doi.org/10.1016/j.actamat.2009.06.049.
[35] Y. Chivel, New approach to multi-material processing in selective laser melting, Phys. Procedia 83 (2016) 891–898, https://doi.org/10.1016/j.phpro.2016.08.093.
[36] J. Koopmann, J. Voigt, T. Niendorf, Additive manufacturing of a steel-ceramic multi-material by selective laser melting, Metall. Mater. Trans. B 50 (2019) 1042–1051, https://doi.org/10.1007/s11663-019-01523-1.
[37] Y. Sakakibara, K. Kubushiro, Stress evaluation at the maximum strained state by EBSD and several residual stress measurements for plastic deformed austenitic stainless steel, World J. Mech. 7 (2017) 195–210, https://doi.org/10.4236/wjm.2017.78018.
[38] L. Saraf, Kernel average misorientation confidence index correlation from FIB sliced Ni-Fe-Cr alloy surface, Microsc. Microanal. 17 (2011) 424–425, https://doi.org/10.1017/S1431927611002996.
[39] M. Calagnotto, D. Ponge, E. Demir, D. Raabe, Orientation gradients and geometrically necessary dislocations in ultrfine grained dual-phase steels studied by 2D and 3D EBSD, Mat. Sci. Eng. A 527 (2010) 2738–2746, https://doi.org/10.1016/j.msea.2010.01.004.
[40] J. Hou, Q.J. Peng, Z.P. Lu, T. Shoji, J.Q. Wang, E.–H. Han, W. KE, Effects of cold working degrees on grain boundary characters and strain concentration at grain boundaries in Alloy 600, Corros. Sci. 53 (2011) 1137–1142, https://doi.org/10.1016/j.corsci.2010.11.022.
[41] D.J. –Badiola, A.I. –Mendia, I. Gutierrez, Study by EBSD of the development of the substructure in a hot deformed 304 stainless steel, Mat. Sci. Eng. A 394 (2005) 445–454, https://doi.org/10.1016/j.msea.2004.11.049.
[42] M. Terner, T.–A. Bayarsaikhan, H.–U. Hong, J.–H. Lee, Influence of gas metal arc welding parameters on the bead properties in automatic cladding, J. Korean Weld. Join. Soc. 35 (2017) 16–25, https://doi.org/10.5781/JWJ.2017.35.1.16.
[43] T. Debroy, H.L. Wei, J.S. Zuback, T. Mukherjee, J.W. Elmer, J.O. Milewski, A.M. Beese, A. Wilson-Heid, A. De, W. Zhang, Additive manufacturing of metallic components-Process, structure and properties, Prog. Mater. Sci. 92 (2018) 112–224, https://doi.org/10.1016/j.pmatsci.2017.10.001.
[44] J.Y. Lee, S.H. Ko, D.F. Farson, C.D. Yoo, Mechanism of keyhole formation and stability in stationary laser welding, J. Phys. D Appl. Phys. 35 (2002) 1570–1576, https://doi.org/10.1088/0022-3727/35/13/320.
[45] E. Akman, A. Demir, T. Canel, T. Sinmazçelik, Laser welding of Ti6Al4V titanium alloys, J. Mater. Process. Technol. 209 (2009) 3705–3713, https://doi.org/10.1016/j.jmatprotec.2008.08.026.
[46] X. Su, Y. Yang, J. Liu, Theoretical study on overlapping mechanism in SLM based on interlayer-staggered scan strategy, Appl. Mech. Mater. 44 (2010) 1482–1486, https://doi.org/10.4028/www.scientific.net/AMM.44-47.1482.
[47] E.R. Denlinger, P. Michaleris, Effect of stress relaxation on distortion in additive manufacturing process modeling, Addit. Manuf. 12 (2016) 51–59, https://doi.org/10.1016/j.addma.2016.06.011.
[48] D. Texier, D. Monceau, Z. Hervier, E. Andrieu, Effect of interdiffusion on mechanical and thermal expansion properties at high temperature of a MCrAlY coated Ni-based superalloy, Surf. Coat. Tech. 307 (2016) 81–90, https://doi.org/10.1016/j.surfcoat.2016.08.059.
[49] J.S. Bartlett, X. Li, An overview of residual stresses in metal powder bed fusion, Addit. Manuf. 27 (2019) 131–149, https://doi.org/10.1016/j.addma.2019.02.020.
[50] L.E. Murr, S.M. Gaytan, D.A. Ramirez, E. Martinez, J. Hernandez, K.N. Amato, P.W. Shindo, F.R. Medina, R.B. Wicker, Metal fabrication by additive manufacturing using laser and electron beam melting technologies, J. Mater. Sci. Technol. 28 (2012) 1–14, https://doi.org/10.1016/S1005-0302(12)60016-4.